Chinese Journal of Aeronautics, (2014),27(1): 160–168

Chinese Society of Aeronautics and Astronautics
& Beihang University

Chinese Journal of Aeronautics

cja@buaa.edu.cn
www.sciencedirect.com

Description of shape characteristics through Fourier and wavelet analysis

Yuan Zhanwei, Li Fuguo *, Zhang Peng, Chen Bo

State Key Laboratory of Solidification Processing, Northwestern Polytechnical University, Xi'an 710072, China

Received 20 January 2013; revised 11 March 2013; accepted 6 May 2013
Available online 1 August 2013

KEYWORDS

Fourier analysis;
Roughness measurement;
Shape characteristics;
Similarity;
Wavelet analysis

Abstract In this paper, Fourier and Wavelet transformation were adopted to analyze shape characteristics, with twelve simple shapes and two types of second phases from real microstructure morphology. According to the results of Fast Fourier transformation (FFT), the Fourier descriptors can be used to characterize the shape from the aspects of the first eight Normalization amplitudes, the number of the largest amplitudes to inverse reconstruction, similarity of shapes and profile roughness. And the Diepenbroek Roughness was rewritten by Normalization amplitudes of FFT results. Moreover, Sum Square of Relative Errors (SSRE) of Wavelet transformation (WT) signal sequence, including approximation signals and detail signals, was introduced to evaluate the similarity and relative orientation among shapes. As a complement to FFT results, the WT results can retain more detailed information of shapes including their orientations. Besides, the geometric signatures of the second phases were extracted by image processing and then were analyzed by means of FFT and WT.

1. Introduction

Shapes with associated features such as size, shape, profile roughness (boundary irregularity) and orientation have drawn extensive attention in the scientific studies.[1–7] For example, in material studies, the shape characteristics of second phases and particles have been regarded as important factors affecting materials mechanical behavior.[8]

Features such as size, shape, profile roughness and orientation can be estimated by the equivalent diameter, shape factor, fractal dimension and Feret angle.[1,9] In the past decades, researchers have proposed various methods of studying and categorizing shape characteristics.[1,3–7,10] Hentschel and Page[1] have identified redundant descriptors for shape characteristics such as aspect ratio and the square root of form factor, with each descriptor sensitive to a different attribute of shape elongation and ruggedness, respectively. Zhang and Lu[5] have classified and reviewed a variety of methods of shape representation and description techniques from both contour-based methods and region-based methods. Through multi-scale fractal dimension, Backes and Bruno[3] have successfully represented and characterized shape contour in a dynamic evolution context. What's more, artificial neural network has been introduced by Clark et al.[11] to identify the shape features of

* Corresponding author. Tel.: +86 29 88474117.
E-mail address: fuguolx@nwpu.edu.cn (F. Li).

Peer review under responsibility of Editorial Committee of CJA.

ELSEVIER Production and hosting by Elsevier

1000-9361
http://dx.doi.org/10.1016/j.cja.2013.07.011

plants. Still, balance between accuracy and efficiency for shape description should be met with appropriate descriptors.

Among these techniques, spectrum analysis as an effective tool with many advantages, such as being simple to compute, overcoming the problem of noise sensitivity and boundary variations, has been utilized widely in shape description.[5] Drevin[6] have used the Fourier transform results to determine roundness of particles. Kindratenko et al.[12] have applied Fourier and fractal analyses to describe the shape of micro particles from microscope images. Li et al.[13] have analyzed the irregularity of graphite nodules of ductile iron in one-, two- and three-dimensional space. Through the utilization of a Fourier–wavelet representation, Lestrel et al.[14] have characterized 2D shape features within biological sciences. Though plenty of works have been done by means of the above studies, seldom of them is related to the influence of analyzed shape orientation and shape axis ratio on spectrum analysis results.

In this paper, with different types of simple shapes, shape characteristics including shape similarity, influence of orientation, shape axis ratio and profile roughness have been processed by using both Fourier transformation (FT) and Wavelet transformation (WT) in Sections 3 and 4. Besides, the application of spectrum analysis to the second phases from real microstructure morphology is shown in Section 5.

2. Methodology

2.1. Extracting geometric signature

The analysis of this study can be divided into two parts as twelve simple shapes and the second phases from real microstructure morphology. In the first part, simple shapes are selected to analyze the circle, ellipse, triangle, square and rectangle, with the same equivalent diameter ED = 50 (ED = $4\pi A/P$, P, perimeter; A, shape area). Specified shape parameters are: circle, ellipse (1:1.5) (1:1.5, meaning the ratio of length of axis or side at horizontal to vertical, the same as below), ellipse (1:2), ellipse (2:1), ellipse (1:3), equilateral triangle (triangle-1), and its rotated 60° relative to triangle-1 (triangle-2), square (square-1), and with a rotation 45° (square-2), rectangle (2:1), rectangle (1:2), and rectangle (1:3). In the second part, two second phases are from the real microstructure morphology.

As for spectrum analysis, the geometric signature should be firstly extracted from shapes.[5,6] With regard to simple shapes, their centroids are easy to be determined, while the centroids of the second phases have to be calculated by image processing (which is discussed at length in Section 5). Then, geometric signatures of shape profiles are extracted by radial vectors originating from the centroid and terminating at the boundary of the shape sweeping through 360°, starting from x axis along the counter-clockwise (as shown in Fig. 1). In this research, 128 (2^7) radial measurements are chosen with an angle increment by 2.8125°, which is prepared as shape geometric signature for the following analysis.

2.2. Fourier transformation (FT)

Fourier transformation is a procedure of high efficiency for spectrum analysis of a time series, especially for processing signals. In essence, it is a way to decompose the limited signal $f(t)$

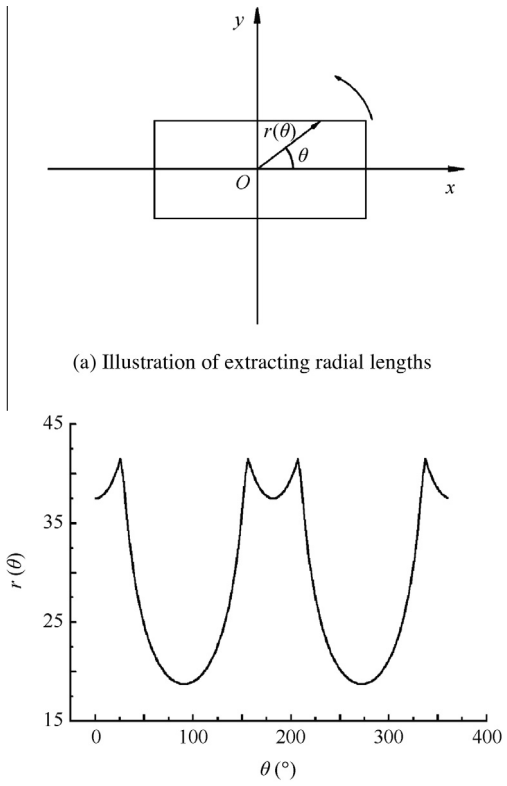

Fig. 1 Extracting geometric signature of a rectangle.

to the space based on orthogonal vector $\{e^{iwt}\}$(i is the square root of -1, w is period parameter), and the transformation equations are as follows:

$$F(w_1, w_2) = \sum_{m=-\infty}^{\infty}\sum_{n=-\infty}^{\infty} f(m,n)e^{-jw_1 m}e^{-jw_2 n} \tag{1}$$

In the above equation, w_1, w_2 and m, n are the period and space parameters, respectively. $F(w_1,w_2)$ is the Fourier space representation of $f(m,n)$ with its discrete form as

$$F(p,q) = \sum_{m=0}^{M-1}\sum_{n=0}^{N-1} f(m,n)e^{-j\frac{2\pi mp}{M}}e^{-j\frac{2\pi nq}{N}} \tag{2}$$

where $p = 0,1,\ldots,M-1$; $q = 0,1,\ldots,N-1$.

In terms of the adopted Fast Fourier Transformation (FFT) method, the efficiency of FT has been greatly improved within a wide range of application, including spectral analysis, signal processing and Fourier spectroscopy. According to FFT analysis, the amplitude can be written as follows:

$$F(u) = R(u) + jI(u) \tag{3}$$

$$A_u^S = \frac{\|\boldsymbol{F}_u^S\|}{\|\boldsymbol{F}_0^S\|} \quad u = 1,2,\ldots,N-1 \tag{4}$$

where $R(u)$ and $I(u)$ are the real and imaginary parts of the transforming data; j is the square root of -1. A_u^S stands for the Normalization amplitude, while $\|\boldsymbol{F}_u^S\|$ indicates the amplitude of $F(u)$, and $\|\boldsymbol{F}_0^S\|$ is the amplitude of the 0th Fourier Descriptor.

2.3. Wavelet transformation (WT)

Wavelet transformation is of multi-resolution characteristics which can decompose the signals into time segments in high frequency domain, and frequency subdivision in low frequency domain through signal (function) translation operations. According to the requirement of analysis, any details in a signal can be focused on. Through WT, the limited signal $f(t)$ can be decomposed to the space W_{-j} $(j = 1,2,\ldots,J)$ and V_{-j} $(j = 1,2,\ldots,J)$. By applying the proper basic wavelet, the detailed information of signals in the time domain and frequency domain can be obtained. The equations for Wavelet transformation are as follows:

$$\mathrm{WT}_f(a,b) = \frac{1}{\sqrt{|a|}} \int_R f(t)\phi\left(\frac{t-b}{a}\right)\mathrm{d}t \tag{5}$$

In which, $\mathrm{WT}_f(a,b)$ are the wavelet coefficients, and $\phi\left(\frac{t-b}{a}\right)$ is the mother wavelet function. a and b are the dyadic dilation and position, respectively. Based on WT results, the approximation signals and detail signals can be reconstructed. The approximation signals represent extracted main characteristic signals, and detail signals stand for extracted detailed information.

In this study, software Origin 8.0 and MATLAB are used to carry out FFT analysis and Wavelet transformation respectively with the extracted geometric signatures.

3. Fourier transformation for simple shapes

3.1. Analysis of FFT results

Because the amplitudes in high frequency (> 0.07 Hz) of FFT results are small, as shown in Figs. 2 and 3, the FFT amplitude and their first eight Normalization amplitudes in frequency ranging from 0 to 0.07 Hz are plotted. For all the twelve shapes of the same equivalent diameter, the 0th amplitudes of FFT results, corresponding to an average magnitude of analyzed signal, are distinct due to the differences among shapes.

The influences of shape orientation, axis ratio and sequence of Normalization amplitude are discussed as follows:

(1) Comparing the Normalization amplitudes among different orientation shapes, namely ellipse (1:2) and ellipse (2:1), triangle-1 and triangle-2, square-1 and square-2, rectangle (2:1) and rectangle (1:2), it is observed that the influence of shape orientation by FFT is little because they have the same amplitude distribution in both magnitudes and the order. In fact, they are the same signal segment with different starting positions. Therefore, they can be translated in the same spectrum (Normalization amplitudes) by FFT.

(2) The FFT results of similar shape type with different axis/side length ratios, namely circle, ellipse (1:1.5), ellipse (1:2), and ellipse (1:3); square, rectangle (1:2), and rectangle (1:3), have been compared in the group. It is found that the circle has single 0th amplitude. Different from circle, the 2nd and the 4th amplitude of ellipses increase gradually along with the decrease of the ratio. The same trend can be seen in rectangles that the 2nd Normalization amplitude rises with the increase of the ratio. This feature may be related to elongation of shapes. Hence, the 2nd Normalization amplitude can be considered as axis ratio index to some extent.

(3) As to non-triangle shapes, the 1st, 3rd, 5th and 7th normalized amplitudes remain the same value 0, while those amplitudes of triangles are distinct, especially of the 3rd one. Also, the 8th normalized amplitudes are salient for triangles and rectangles (including squares), different from circle and ellipses. According to the above results, it may be related to the asymmetry and triangularity of the 1st, 3rd, 5th and 7th Normalization amplitudes, especially the triangularity index of the 3rd one. And the 8th Normalization amplitudes may be related to the squareness of the shapes.

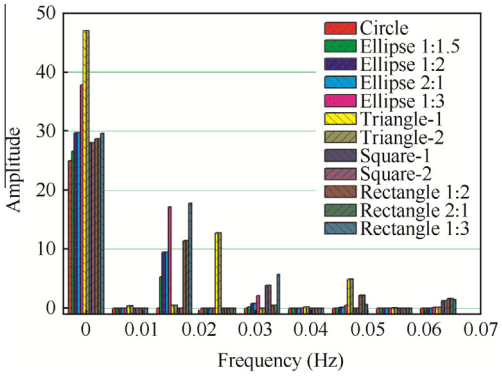

Fig. 2 FFT results of twelve selected simple shapes.

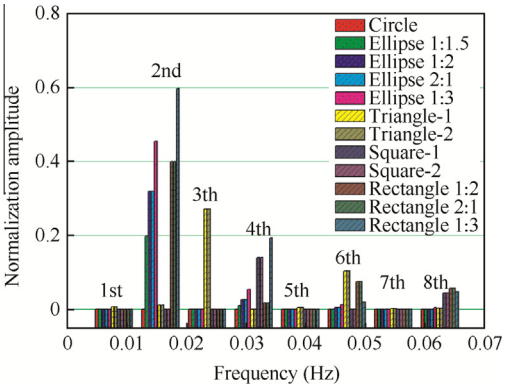

Fig. 3 Normalization amplitude vs. frequency (the amplitude order).

3.2. Similarity of shapes by FFT results

In order to ascertain the difference (or similarity) between the two shapes, a variable D can be used to describe this feature as follows:

$$D = \sqrt{\sum_{u=1}^{M}\left(A_u^I - A_u^J\right)^2} \quad (u = 1,2,\ldots,N-1) \tag{6}$$

In the above equation, A_u^I and A_u^J are the normalized amplitudes of shape I and shape J, respectively. Statistically speaking, the variable D can collect difference between shapes from

normalized amplitudes series. Taken the difference between ellipses to circle as an example, the calculated results are 0.1972 for ellipse (1:1.5) to circle, 0.3208 for ellipse (1:2) to circle, 0.4585 for ellipse (1:3) to circle. With aspect ratio increasing, the similarities of ellipses to circle are getting worse.

3.3. Inverse Fast Fourier Transform (IFFT)

The aim of FFT is to obtain a series of Fourier descriptors for input signals. Actually, one Fourier descriptor is not enough to quantitatively identify an analyzed signal. Here, Inverse Fast Fourier Transform (IFFT) is applied to determining how many the first largest FFT harmonics (sequenced from the great magnitude harmonics to the smaller ones) are needed to reconstruct the shape signal. The total Sum of the Square of Relative Errors (SSRE) is introduced to estimate the differences between original shape and reconstructed shape by IFFT as follows:

$$\mathrm{SSRE} = \sqrt{\sum_{i=1}^{M}\left(\frac{r_i^{\mathrm{IFFT}}(\theta) - r_i^{o}(\theta)}{r_i^{o}(\theta)}\right)^2} \tag{7}$$

where $r_i^{o}(\theta)$ is the ith original measurement for accumulative angle θ, and $r_i^{\mathrm{IFFT}}(\theta)$ is the ith original measurement for accumulative angle θ of IFFT results.

Fig. 4 shows the SSRE between original shape measurements and obtained shape measurements, which is from IFFT by using the first several largest Fourier descriptors. As the number of first largest Fourier descriptors increases, the decrease of SSRE implies higher accuracy by means of IFFT approach. Among the given shapes, rectangle (1:3) and triangles are not prone to be reconstructed with a few largest harmonics. Generally speaking, less than ten largest Fourier descriptors can reconstruct the twelve given shapes by IFFT with SSRE $<15\%$, which coincides with the results of Ref. 15.

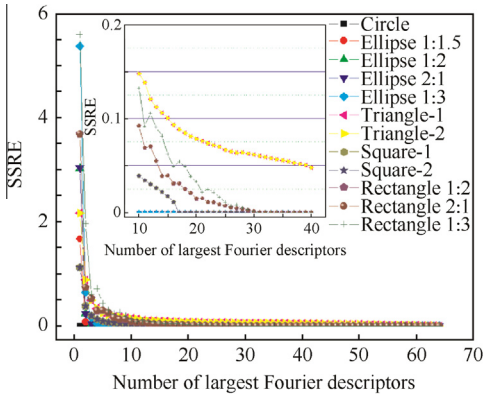

Fig. 4 Correlation between SSRE and the number of the first several largest Fourier descriptors by IFFT reconstruction. Inset: details ranging from 10 to 40.

3.4. Profile roughness

In terms of shapes profile roughness, Diepenbroek has adopted the first twenty-four coefficients (Fourier descriptors) of Fourier transformation results to make description.[6,16] The equation was given as

$$R = \frac{\sqrt{0.5\sum_{u=1}^{k}(R^2(u) + I^2(u))}}{\sqrt{(R^2(0) + I^2(0))}} \tag{8}$$

where $R(0)$ and $I(0)$ is the Fourier 0th real and imaginary amplitude. To simplify this equation with the inspiration of Eqs. (6) and (8) can be rewritten as

$$R = \sqrt{\sum_{u=1}^{M}(A_u^S - A_u^C)^2} \quad (u = 1, 2, \ldots, N-1) \tag{9}$$

where A_u^S is the uth normalized amplitude of Fourier descriptors for shape S, and A_u^C is the uth normalized amplitude of Fourier descriptors of circle. This can be explained that circle is generally considered as the epitome of a smooth shape and single 0th FFT amplitude. From Eq. (9), it can be found that the profile roughness of selected shapes is relative to circle, and similar to Eq. (6) without coefficient $\sqrt{0.5}$. In addition, it eliminates the effect of shape size, and only focuses on the irregularity of shape boundary.

In Table 1, three different roughness results are shown as Diepenbroek Roughness (DR), Normalization Amplitude Roughness (NAR) and Shape Factor (SF) which is the most sensitive one to the boundary irregularity (Shape Factor: $F = P^2/(4\pi A)$, P, perimeter; A, area of the shape, reciprocal of form factor[1]). The result of triangle is a little less than that of rectangle (1:3) from SF results, while there exist dramatic differences among the results of DR or NAR. The SF and DR (or NAR) results between ellipse (1:3) and triangle are different because SF of triangle is greater than that of ellipse (1:3), and is opposite to DR (or NAR) results. This may be due to the deviation of radial measurements because ellipse (1:3) is more serrated than that for the triangle.

According to the above analysis, it can be observed that the shape characteristics can be comprehensively described by FFT results. The size of shapes and boundary irregularity can be reflected by FFT amplitude; the FFT amplitudes distribution can reveal the asymmetry, triangularity and squareness of shapes. Moreover, the main features of shapes can be distinguished through FFT for some similar shapes such as rectangles and ellipses. However, there are some difficulties in accurately differentiating shape orientation by means of FFT results.

Table 1 Profile roughnesses of twelve simple shapes from FFT results and shape factor.

Material	Shape parameters		
	DR	NAR	SF
Circle	0	0	1
Ellipse 1:1.5	0.1394	0.1972	1.063
Ellipse 1:2	0.2268	0.3208	1.1902
Ellipse 2:1	0.2268	0.3208	1.1902
Ellipse 1:3	0.3242	0.4585	1.5179
Triangle-1	0.2124	0.3004	1.654
Triangle-2	0.2124	0.3004	1.654
Square-1	0.1057	0.1494	1.2732
Square-2	0.1057	0.1494	1.2732
Rectangle 1:2	0.2918	0.4127	1.4324
Rectangle 2:1	0.2918	0.4127	1.4324
Rectangle 1:3	0.4483	0.6339	1.6977

4. Wavelet transformation for simple shapes

4.1. Analysis of WT results

As shown in Fig. 5(a), the approximation signals from low frequency information is plotted, reflecting the main characteristics of the shapes with 4 layers from a_1 to a_4. In Fig. 5(b), detail signals from high frequency information with 4 layers ranging from d_1 to d_4 are depicted.

Based on the results of WT, it can be observed that approximation signals of circle, ellipses, square and rectangles show different features which can be applied to classifying the shape types at the first stage. For instance, while studying the results of WT for rectangle and ellipse, it can be found that for the main characteristic signals, differences can be found from the 1st layer (a_1) to the 3rd layer (a_3), while the 4th layer signals (a_4) are almost the same. This may be because that further approximation signals (a_4) reflect the shapes' original type.

In terms of the same shapes with different orientations such as ellipse (1:2) and ellipse (2:1), triangle-1 and triangle-2, square-1 and square-2, and rectangle (1:2) and rectangle (2:1), it can be observed that the main characteristic signals revolve a certain angle between the same shapes because of their different orientations. For instance, there exists a difference of orientation angle 90° between ellipse (1:2) and ellipse (2:1).

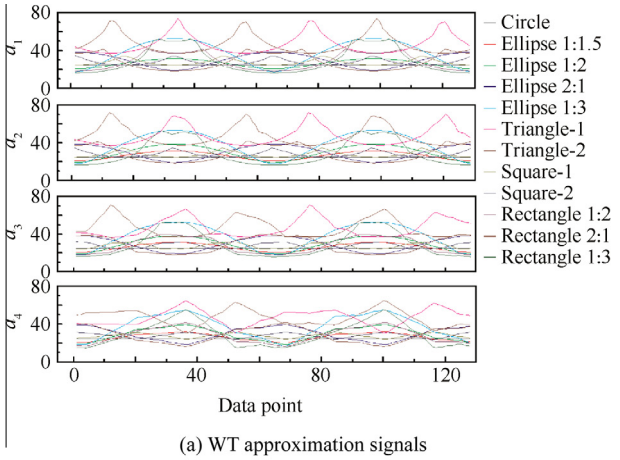

(a) WT approximation signals

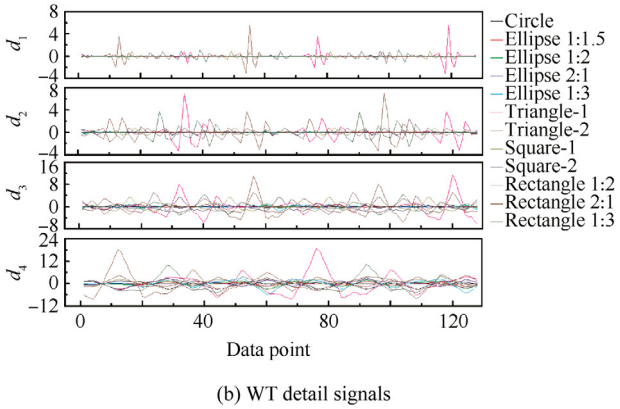

(b) WT detail signals

Fig. 5 Results of WT analysis for the given twelve simple shapes.

Additionally, detail signals of these shapes demonstrate the same characteristics.

As the ratio of axis/side length increases, the approximation signals and detail signals of ellipses remain the same in characteristics. Also, differences can be detected when the maximum amplitude of approximation signals and detail signals increase as the ratio of axis/side length rises. However, the trends in the quadrangle group including square-1, rectangle (1:2) and rectangle (1:3) are different for both approximation signals and detail signals. Besides, the distribution of a4 signals of ellipses group changes gradually into two-peaks as the ratio of axis/side length increases, and the same trend can be found for quadrangle as well.

4.2. Similarity of shapes by WT results

In order to quantitatively describe the similarity of the two shapes, Fourier descriptors by Eq. (6) can be adopted. WT results can be employed as well. For two similar signals with different orientations (such as square-1 and square-2), the differences in orientation can be determined by using the minimum Sum of Squares of Relative Error (SSRE) between the two signals after one of them translating a certain angle θ ($0 \leqslant \theta < 360°$). Still, the above case is only considered when the two signals are in the similar amplitude range. If the same signals were amplified or offset, the desired results would not be obtained by using the above mentioned method. As a result, these signals need to be normalized by employing the maximum amplitude, which is also an indicator for size ratio of the two signals.

As for Normalization signals, SSRE of signal translation θ' and size ratio can be calculated respectively by

$$Nr_i(\theta) = \frac{r_i(\theta)}{\max(r_i(\theta))} \tag{10}$$

$$\mathrm{SSRE}_j^i(\theta') = \sqrt{\sum_{i=1}^{M}\left(\frac{Nr_i(\theta+\theta') - Nr_j(\theta)}{Nr_j(\theta)}\right)^2} \tag{11}$$

$$\mathrm{SR}_j^i = \frac{\max(r_i(\theta))}{\max(r_j(\theta))} \tag{12}$$

In the above equations, $r_i(\theta)$ is the signal sequence for accumulative angle θ, and max $(r_i(\theta))$ represents the maximum amplitude of signal sequence $r_i(\theta)$. $Nr_i(\theta + \theta')$ demonstrates the normalized signal sequence $Nr_i(\theta)$ after translation $\theta'(0 \leqslant \theta' < 360°)$. $\mathrm{SSRE}_j^i(\theta')$ is a series of the sum of squares of relative errors of signal sequence i after translation θ' to signal sequence j. SR_j^i represents relative size ratio between signal sequence i and signal sequence j.

Through computing SSRE of the two signals, the relative position of the two shapes can be demonstrated by the minimum $\mathrm{SSRE}_j^i(\theta')$ with signal translation θ'.

Besides, the number of the minimum SSRE can be applied to indicating the shape symmetry, with the same sequence i and j. Here, the similarities of ellipses are calculated by using the approximation signal a1. The results are as follows: two symmetry positions for ellipse (1:1.5) itself at 0 and π; two minimum $\mathrm{SSRE}_j^i(\theta')$ values of 1.456 for ellipse (1:2) to ellipse (1:1.5) at 0 and π; two minimum $\mathrm{SSRE}_j^i(\theta')$ values of 2.795 for ellipse (1:3) to ellipse (1:1.5) at 0 and π.

5. Application in material science

5.1. Extracting geometric signatures

In order to use FFT and WT, the geometric signatures should be extracted firstly from the phase of Titanium alloy and SiC particle in SiCp/Al composites, as shown in Figs. 6(a) and 7(a). Images smoothing and binarization have been processed to differ the second phases from matrix. A smooth shape edge has been obtained by means of dilation and erosion processing as shown in Figs. 6 and 7.

The calculation of shape centroid coordinates by using the image processing function of MATLAB software:

(1) In binary images, the images are presented by a matrix with 0 and 1 only, where "1" represents the pixel in prospect, and "0" stands for the pixels in background. The coordinates of each pixel in prospect are recorded by abscissa i and ordinate j, as shown in Fig. 6(c).

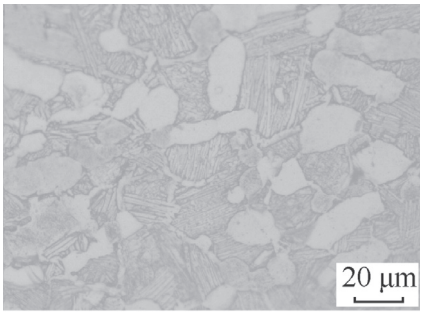

(a) Titanium alloy microstructure

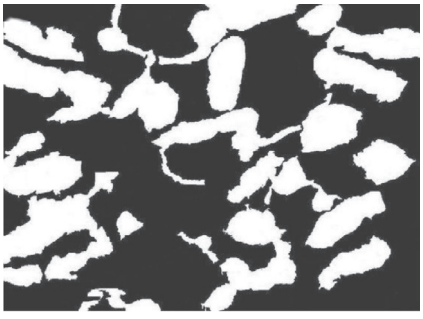

(b) Binary image

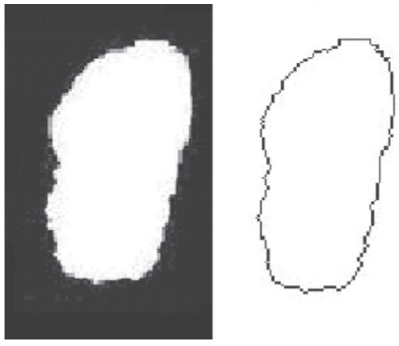

(c) Selected titanium alloy phase

Fig. 6 Titanium alloy microstructure and images.

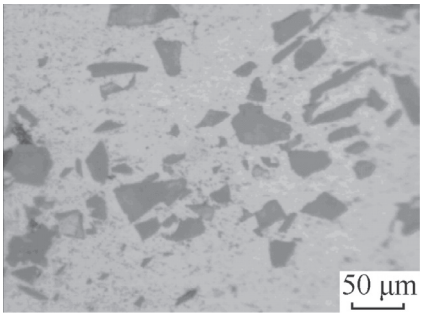

(a) SiCp/Al microstructure

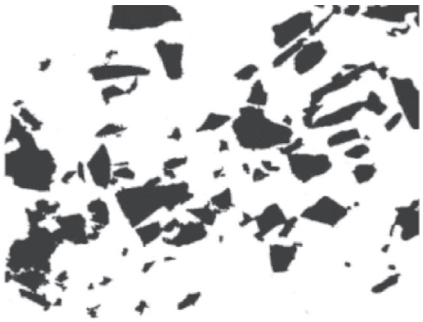

(b) Binary image

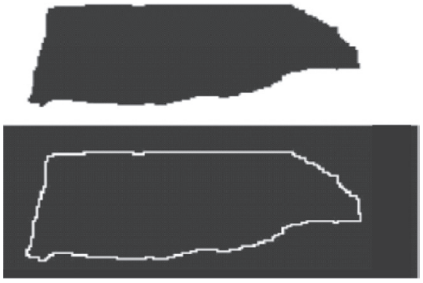

(c) Selected SiC particle

Fig. 7 SiCp/Al microstructure and image.

(2) Set the quality of pixels in prospect as 1, namely $f(i, j) = 1$.

(3) The total quality for all pixels in prospect is counted:

$$M(0,0) = \sum_{i,j \in S} f(i,j)$$

(4) Calculate the first order torque, $M(1, 0)$ and $M(0, 1)$ for i and j, respectively:

$$M(1,0) = \sum_{i,j \in S} if(i,j)$$

$$M(0,1) = \sum_{i,j \in S} jf(i,j)$$

(5) Calculate shape centroid coordinates, with m denoting abscissa coordinate, and n denoting ordinate coordinate of centroids:

$$m = M(1,0)/M(0,0)$$

$$m = M(0,1)/M(0,0)$$

The extraction of geometric signatures:

(1) Show the second phase edge only, extract the pixel in prospect where the adjacent pixels are at least with a value "0", and record the pixel coordinates.
(2) Record radial measurements by radial vector originating from the centroid and terminating at the outlines of the shape sweeping through 360° from x axis along the counter-clockwise. 128 radial measurements are extracted as the simple shapes above.

5.2. Spectrum analysis

According to Fig. 6(a), the shape type of the selected phase in Titanium alloy looks like ellipse or rectangle with distinct symmetry, while the edge is not smooth. The shape type of the selected SiC particle is much like rectangle with low symmetry, as shown in Fig. 7(a). However, the edge of the particle is a little smoother than that of the selected phase in Titanium alloy. As to the extracted geometric signatures, the FFT and WT results of the two shapes are processed and shown in Fig. 8. It can be found that the amplitudes are salient in the range of 0–0.1 Hz, especially for the 1st and 2nd normalized amplitude from FFT results. In contrast to the FFT results of the above simple shapes, these two shapes are close to ellipse (1:3) or rectangle (1:2). Still, there exist some differences such as the 1st and 3rd normalized amplitude of FFT results of the selected Titanium alloy phase, and SiC particles are especially greater than ellipse (1:2) or rectangle (1:3) with lower symmetry of these two shapes than ellipse (1:2) or rectangle (1:3). Besides, the 1st FFT normalized amplitude for the Titanium alloy phase is greater than that of SiC, which can be supported by WT results that detail signal d1 layer of the Titanium alloy phase is more serrated.

Concerning WT results, it can be found that the approximation signals of the selected Titanium alloy phase are more similar to ellipse (1:2). Although, approximation signals a_4 of SiC particle are similar to rectangle (2:1) and ellipse (2:1), a_1, a_2 and a_3 are much more close to ellipse (2:1). As for detail signals, d_4 is close to ellipse (2:1) while d_1 and d_2 are different. The roughness of the two shapes has also been calculated as shown in Table 2. The DR or NAR results of the selected Titanium alloy phase are a little greater than those of the selected SiC particle, while SF shows reverse results. This difference may be due to the definition of SF from the area and the perimeter of shapes. According to Figs. 6(c) and 7(c), the edge of the selected Titanium alloy phase is much more serrated than that of the selected SiC particle, which can be reflected by the FFT results more comprehensively.

In the study of material science, the simple shapes are usually utilized to represent the analyzed shapes or particles in order to simplify the computation such as geometrical model in numerical simulation.[17,18] In accordance with observation of these two shapes, they are close to ellipse or rectangle. Using Eq. (6), the difference (or similarity) between selected shapes and selected simple shapes are calculated. The minimum SSRE of original signals and approximation signals (from a_1 to a_4) of the selected shapes are shown as well by using Eqs. (10) and (11). In Table 3, the selected Titanium alloy phase is close to ellipse (1:2), and SiC particle with lower difference (high similarity) to rectangle (1:2) from FFT results. Both the minimum SSRE of original signals and approximation signals of Titanium alloy phase indicate that it is more close to rectangle (1:3) than the other selected shapes. While in Table 4, SiC

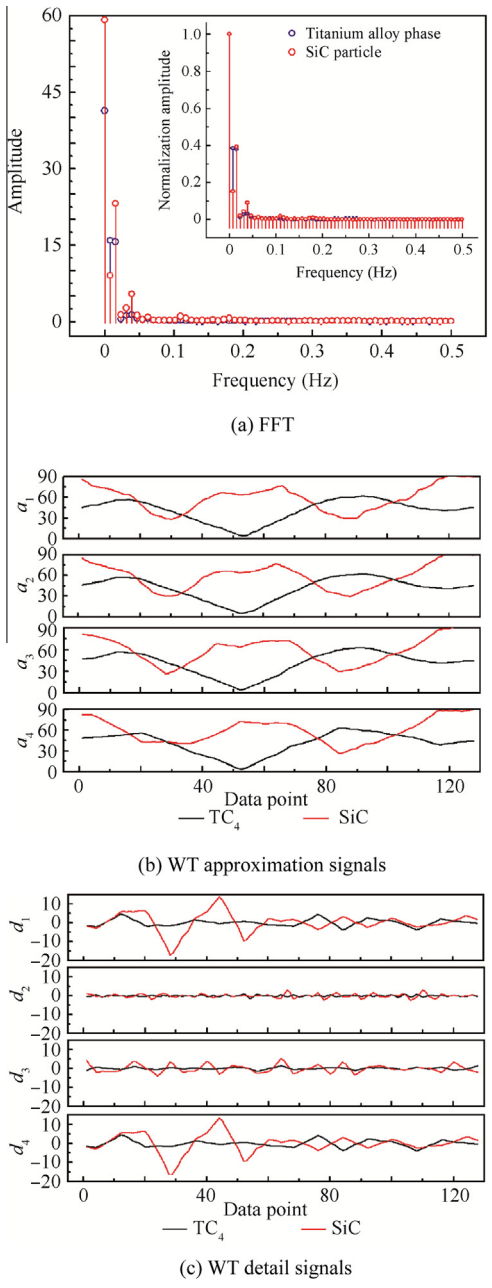

Fig. 8 Results of spectrum analysis for the selected Titanium alloy phase and selected SiC particle.

Table 2 Profile roughnesses of the second phases by FFT and shape factor.

Material	Shape parameters		
	DR	NAR	SF
Titanium alloy phase	0.3833	0.5421	1.2010
SiC particle	0.3073	0.4346	1.8749

Table 3 Similarities between the Titanium alloy phase and the selected simple shapes.

Material	Original	FFT	WT			
			a_1	a_2	a_3	a_4
Ellipse 1:2	12.7846	0.3909	12.8183	12.4051	12.6634	13.676
Ellipse 1:3	8.1740	0.3944	8.1911	7.9212	8.2093	8.7717
Rectangle 1:2	10.8695	0.3944	10.8613	10.5545	11.2094	11.0685
Rectangle 1:3	7.2275	0.4788	7.2608	6.9272	7.0119	7.2218

Table 4 Similarities between the SiC particle and the selected simple shapes.

Material	Original	FFT	WT			
			a_1	a_2	a_3	a_4
Ellipse 1:2	3.7104	0.1967	3.5428	3.5423	3.4148	3.003
Ellipse 1:3	2.3053	0.1973	2.1885	2.1827	2.0842	2.1513
Rectangle 1:2	2.4574	0.1930	2.322	2.3535	2.5248	2.0078
Rectangle 1:3	2.7561	0.1959	2.7945	2.8136	2.8330	3.0163

particle is much alike to ellipse (1:3) from original signals to a_3, though there is little variation for a_4. Based on the above analysis, there exist differences between the FFT and WT results of the selected shapes. This may be because that the FFT results only focus on frequency domain information while WT results reserve time domain and frequency domain information.[5,19,20] Hence, minimum SSRE of original signals and approximation signals is a more appropriate tool to trace the similarity between shapes when it focuses on the shape profiles.

6. Conclusions

Through Fourier and Wavelet transformation, two types of shapes including twelve simple shapes and two selected second phases in real microstructure morphology were analyzed respectively.

(1) By comparing the FFT results of simple shapes, it can be found that different shapes led to various FFT results, which could be applied to characterizing particle patterns such as profile roughness and similarity. The first eight Normalization amplitudes and the number of the largest amplitudes were analyzed. The Diepenbroek Roughness was rewritten by Normalization amplitudes of FFT results.
(2) Through WT analysis, the Squares of Relative Errors (SSRE) of Wavelet transformation signal sequences including the approximation signals and detail signals can be used to estimate the orientation and symmetry of shapes. As a complement to FFT results, the WT results retain more detailed information of shapes including their orientations.
(3) In contrast to the FFT results of simple shapes, the selected Titanium alloy phase was close to ellipse (1:2), and SiC particle was much similar to rectangle (1:2). However, from minimum SSRE of original signals and WT approximation signals, the Titanium alloy phase was much closer to rectangle (1:3) and SiC particle was alike ellipse (1:3).

Acknowledgements

The authors are very grateful for the support received from the National Natural Science Foundation of China (No. 51275414) and the Aeronautical Science Foundation of China (No. 2011ZE53059).

References

1. Hentschel ML, Page NW. Selection of descriptors for particle shape characterization. *Part Part Syst Char* 2003;**20**(1):25–38.
2. Loncaric S. A survey of shape analysis techniques. *Pattern Recogn* 1998;**31**(8):983–1001.
3. Backes AR, Bruno OM. Shape classification using complex network and multi-scale fractal dimension. *Pattern Recogn Lett* 2010;**31**(1):44–51.
4. El-ghazal A, Basir O, Belkasim S. Farthest point distance: a new shape signature for Fourier descriptors. *Signal Process Image Commun* 2009;**24**(7):572–86.
5. Zhang D, Lu G. Review of shape representation and description techniques. *Pattern Recogn* 2004;**37**(1):1–19.
6. Drevin GR. Computational methods for the determination of roundness of sedimentary particles. *Math Geol* 2006;**38**(7):871–90.
7. Cope JS, Corney D, Clark JY, Remagnino P, Wilkin P. Plant species identification using digital morphometrics: a review. *Expert Syst Appl* 2012;**39**(8):7562–73.
8. Bozic D, Dimcic B, Dimcic O, Stasic J, Rajkovic V. Influence of SiC particles distribution on mechanical properties and fracture of DRA alloys. *Mater Design* 2010;**31**(1):134–41.
9. Jennings B, Parslow K. Particle size measurement: the equivalent spherical diameter. *Proc R Soc Lond A Math Phys Sci* 1988;**419**(1856):137–49.
10. Xu J, Faruque J, Beaulieu CF, Rubin D, Napel S. A comprehensive descriptor of shape: method and application to content-based retrieval of similar appearing lesions in medical images. *J Digit Imaging* 2012;**25**(1):121–8.
11. Clark JY, Corney DP, Tang HL. Automated plant identification using artificial neural networks. In: Computational Intelligence in Bioinformatics and Computational Biology (CIBCB); 2012. p. 343–8.
12. Kindratenko VV, Van Espen PJM, Treiger BA, Van Grieken RE. Characterisation of the shape of microparticles via fractal and

Fourier analyses of scanning electron microscope images. *Microchim Acta* 1996;**13**:355–61.
13. Li J, Lu L, Lai MO. Quantitative analysis of the irregularity of graphite nodules in cast iron. *Mater Charact* 2000;**45**(2):83–8.
14. Lestrel PE, Cesar Jr RM, Takahashi O, Kanazawa E. A Fourier–wavelet representation of 2-D shapes: sexual dimorphism in the Japanese cranial base. *Anthropol Sci* 2004;**112**(1):3–28.
15. Hearn DJ. Shape analysis for the automated identification of plants from images of leaves. *Taxon* 2009;**58**(3):934–54.
16. Diepenbroek M, Bartholomä A, Ibbeken H. How round is round? A new approach to the topic 'roundness' by Fourier grain shape analysis. *Sedimentology* 1992;**39**(3):411–22.
17. Zhang P, Li FG. Microstructure-based simulation of plastic deformation behavior of SiC particle reinforced Al matrix composites. *Chin J Aeronaut* 2009;**22**(6):663–9.
18. Chawla N, Chawla K. Microstructure-based modeling of the deformation behavior of particle reinforced metal matrix composites. *J Mater Sci* 2006;**41**(3):913–25.
19. Brown RA, Lauzon ML, Frayne R. A general description of linear time-frequency transforms and formulation of a fast, invertible transform that samples the continuous S-transform spectrum nonredundantly. *IEEE Trans Signal Process* 2010;**58**(1):281–90.
20. Huang L, Kemao Q, Pan B, Asundi AK. Comparison of Fourier transform, windowed Fourier transform, and wavelet transform methods for phase extraction from a single fringe pattern in fringe projection profilometry. *Opt Laser Eng* 2010;**48**(2):141–8.

Yuan Zhanwei is a Ph.D. candidate in School of Materials Science and Engineering, Northwestern Polytechnical University. His main research interests lie in shape characterization and mechanical properties of SiCp/Al composites.

Li Fuguo is a professor with Ph.D. degree in State Key Laboratory of Solidification Processing, Northwestern Polytechnical University. His main research interests are integrated technologies of design and control of the forming process for aeronautical materials, as well as process coupling computation method of multi-scale and multi-physics of materials forming process.